ACS APPLIED MATERIALS & INTERFACES

Research Article

www.acsami.org

Adjustment of ON-State Retention Ability Based on New Donor–Acceptor Imides through Structural Tailoring for Volatile Device Applications

Hao Zhuang,[†] Qianhao Zhou,[†] Yang Li,[†] Qijian Zhang,[†] Hua Li,*[,†,‡] Qingfeng Xu,[†,‡] Najun Li,[†,‡] Jianmei Lu,*[,†,‡] and Lihua Wang[†,‡]

[†]College of Chemistry, Chemical Engineering and Materials Science, Collaborative Innovation Center of Suzhou Nano Science and Technology, Soochow University, Suzhou 215123, People's Republic of China

[‡]State Key Laboratory of Treatments and Recycling for Organic Effluents by Adsorption in Petroleum and Chemical Industry, Suzhou 215123, People's Republich of China

Supporting Information

ABSTRACT: In this study, two D-A molecules NACANA and CANACA, based on carbazole (CA) donor and naphthalimide (NA) acceptor, with different D-A arrangement (A-D-A and D-A-D) were synthesized. The photophysical and electrochemical properties, microstructure and memory behaviors of both A-D-A and D-A-D molecules were systematically investigated. The fabricated devices ITO/NACANA or CANACA layer/Al with a simple sandwich configuration both exhibited volatile nature after shutting off the external electric field. Interestingly, NACANA showed ON-state retention time of ca. 12 min, longer than that of CANACA (ca. 6 min). The difference in retention ability of the programmed states could be assigned to the difference of the D-A arrangement. This type of retention ability adjustment by varying the arrangement of donor and acceptor segments may provide a guide of structure design for future organic-based specific memory devices with tunable volatile property.

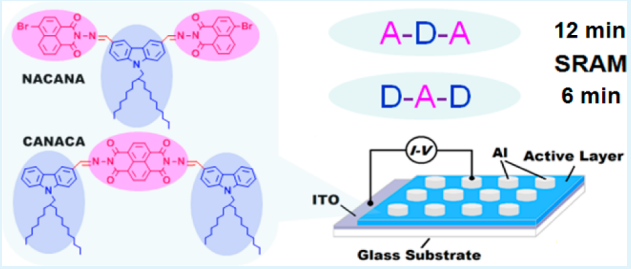

KEYWORDS: *carbazole, donor–acceptor, charge transfer, memory device, SRAM, retention ability*

1. INTRODUCTION

Electro-active materials based on the electron pull-push effect at the molecular level are widely employed in organic electronics due to their merits of low cost, tunable molecular energy level, and vast potential for plastic devices.[1,2] Stimulated by the desire for materials with superior or unique properties, tremendous efforts have been made in the last decades to tune their electronic performance through structural tailoring and have demonstrated good results, such as the variation of the charge transfer functional units,[3] the adjustment of the molecular planarity[4] or conjugation length,[5,6] peripheral decoration,[7,8] or the introduction of specific atoms[9,10] or groups,[11,12] which would influence the molecular levels and the organic film morphology. Recently, as promising alternatives or supplements of the inorganic silicon-based conventional memory, organic memory devices are under extensive investigation in microelectronics.[13−17] A number of studies reported the different memory types (i.e., Write-Once-Read-Many times memory (WORM), Flash memory, Negative Differential Resistance (NDR) effect, Dynamic Random Access Memory (DRAM), Static Random Access Memory (SRAM)) tuned through structure tailoring of the active materials, including the variation in the strength of acceptor groups,[18] the incorporation of bulky pendant moieties,[19] or the adjustment of the flexibility of the spacers[20] between the backbone and the pendent active elements. However, the memory performance tuned by adjusting the D-A arrangement (D-A-D or A-D-A) in donor–acceptor small molecules has rarely been reported.[21] A better understanding of this type of effect is essential for the rational molecular design of future high performance memory devices with desired properties.

The imide-based materials are outstanding candidates owing to their excellent thermal and chemical properties besides the electrical switching behavior.[22,23] Functional imides containing electron donor and acceptor segments in the backbone could readily induce charge transfer that would enhance the conductivity of the active films and was responsible for the observed memory properties.[1,24−26] Therefore, in this paper, we synthesized two imides NACANA and CANACA (Figure 1a) where the electron acceptor naphthalimide (NA) and electron donor carbazole (CA) are linked by hydrazone bonds, considering the advantages that aromatic hydrazones have over other classes of organic semiconductors in terms of high charge carrier mobility and cost-efficient synthesis.[27] In order to prevent the possible poor solubility of our designed imides caused by the NA segment, long branched alkyl chains were

Received: July 2, 2013
Accepted: December 16, 2013
Published: December 16, 2013

   dx.doi.org/10.1021/am405000c | ACS Appl. Mater. Interfaces 2014, 6, 94−100

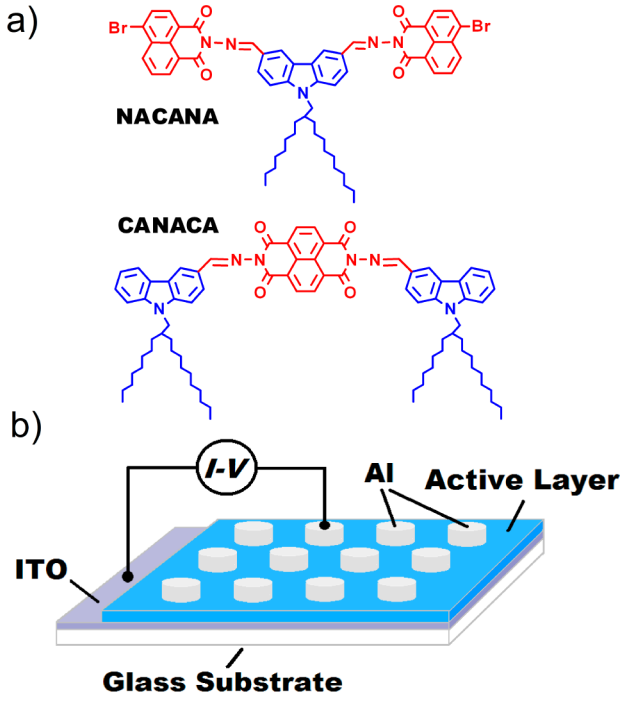

Figure 1. (a) Molecular structure of NACANA and CANACA and (b) scheme of the prototype sandwich device.

incorporated into the molecules on the nitrogen atom. These imides are soluble in several common organic solvents (e.g. chloroform, 1,2-dichloroethane, and chlorobenzene) and possess good film-forming ability. Interestingly, the fabricated sandwich devices (ITO/NACANA or CANACA/Al) were found to possess different ON-state retention ability (i.e., varied retention time for the ON state) though both of them exhibited a volatile nature. The different retention ability of NACANA (ca. 12 min) and CANACA (ca. 6 min) could be essentially attributed to the difference in the D-A arrangement since both molecules have the same electron donor and acceptor segment. We envision this ON-state retention ability adjustment through structural design may provide a useful guide to approach tailored devices with specific data-storage properties in the future.

2. EXPERIMENTAL SECTION

Materials. Carbazole, 2-octyl-1-dodecanol, phosphorus chloride oxide, 1,4,5,8-naphthalenetetracarboxylic dianhydride, hydrazine, and 4-bromonaphthalene anhydride were all purchased from commercial sources (TCI, Alfa Aesar, and Sigma-Aldrich). 1-Bromo-2-octyldodecane was synthesized according to the previous literature.[28] All solvents were purchased from Sinopharm Chemical Reagent Co., Ltd. All the materials were used as received.

Instrumentation and Characterizations. NMR spectra were measured on NMR system 300 MHz and INOVA 400 MHz spectrometers. FT-IR spectra were measured on Varian 3600 FT-IR Fourier Transform Infrared Spectrometer. The elemental analysis was performed on an Italian 1106 FT analyzer. The SEM images were taken on Hitachi S-570 Scanning Electron Microscope. UV−vis absorption spectra were measured at room temperature with a Shimadzu UV-3600 spectrophotometer. Cyclic voltammetry (CV) measurements were performed in 0.1 M acetonitrile solution of tetrabutylammonium perchlorate (TBAP) using a CorrTest CS Electrochemical Workstation equipped with a platinum gauze auxiliary electrode and an Ag/AgCl reference electrode. Atomic force microscopy (AFM) measurements were performed using a MFP-3DTM (Digital Instruments/Asylum Research) AFM instrument. Thermal properties were evaluated from a PE TGA-7 thermogravimetric analysis system (TGA) in a nitrogen atmosphere at a heating rate of 20 °C min^{-1}. XRD measurements were carried out with a Multiple Crystals X-ray Diffractometer (X'Pert PRO, PANalytical). The fabricated devices were characterized under ambient conditions, using a Hewlett-Packard 4145B semiconductor parameter analyzer with Hewlett-Packard 8110A pulse generator. Molecular simulations were carried out with the Gaussian 03 program package. Electronic properties of NACANA and CANACA in the ground state, including molecular orbitals and the electrostatic potential (ESP) surface, were calculated from the density functional theory (DFT): the Becke's three-parameter functional combined with the Lee, Yang, and Parr's correlation functional (B3LYP), along with the 6-31G(d) basis set.

Synthesis of 9-(2-octyldodecyl)-9H-carbazole (ODCA). Carbazole (3.34 g, 20 mmol) and potassium hydroxide (7.0 g) were dissolved in DMF (50 mL), and stirred for 4 h at room temperature. Thereafter, the mixture was heated to 60 °C, and 1-bromo-2-octyldodecane (7.95 g, 22 mmol) was added dropwise. The mixture was stirred for 10 h. After the reaction was completed, the mixture was poured into water and chloroform was used to extract the mixture three times. The collected chloroform solution was then washed with ionized water three times. The chloroform solution was dried with magnesium anhydride for 2 h. Then, the solution was filtered, and chloroform was removed to give honey-colored liquid. The final product was obtained through silica-gel chromatography as colorless oil (5.99 g). Yield: 67%. ^{1}H NMR ($CDCl_3$, 400 MHz), δ (ppm): 8.09 (d, J = 7.7 Hz, 2H), 7.44 (t, J = 7.4 Hz, 2H), 7.38 (d, J = 8.1 Hz, 2H), 7.21 (t, J = 7.6 Hz, 2H), 4.14 (d, J = 7.4 Hz, 2H), 2.04−1.92 (m, 1H), 1.44−1.11 (m, 32H), 0.97−0.77 (m, 6H).

Synthesis of 9-(2-octyldodecyl)-9H-carbazole-3,6-dicarbaldehyde (DAODCA). DMF (dried before use) (8.98 g, 0.12 mol) was placed in a flask in ice bath, and $POCl_3$ (18.84 g, 0.12 mol) was added dropwise in nitrogen atmosphere. Thereafter, the ice bath was removed. ODCA (2.24 g, 5 mmol) was dissolved in 1,2-dichloroethane (25 mL) and added, the temperature was raised to 90°C and the mixture reacted for 48 h. After the reaction was completed, the reaction mixture was poured into water and extracted with chloroform for three times. The collected chloroform solution was washed with ionized water for three times. Then, the solution was dried with magnesium anhydride overnight. Then, the solution was filtered, and the solvent was removed to give black viscous liquid. Pure product was obtained through silica-gel chromatography (CH_2Cl_2/ethyl acetate = 100/1), to give DAODCA as white solid (0.88 g). Yield: 35%. ^{1}H NMR ($CDCl_3$, 400 MHz), δ (ppm): 10.13 (s, 2H), 8.66 (s, 2H), 8.08 (d, J = 7.0 Hz, 2H), 7.52 (d, J = 7.6 Hz, 2H), 4.24 (d, J = 6.8 Hz, 2H), 2.16−2.04 (m, 1H), 1.34−1.10 (m, 32H), 0.92−0.81 (m, 6H).

Synthesis of 9-(2-octyldodecyl)-9H-carbazole-3-carbaldehyde (SAODCA). SAODCA was synthesized during the same reaction process of DAODCA and was obtained as pure product through silica-gel chromatography in yellow liquid (0.37 g). Yield: 16%. ^{1}H NMR ($CDCl_3$, 300 MHz), δ (ppm): 10.11 (s, 1H), 8.62 (s, 1H), 8.15 (d, J = 7.2 Hz, 1H), 8.00 (d, J

dx.doi.org/10.1021/am405000c | ACS Appl. Mater. Interfaces 2014, 6, 94−100

= 7.8 Hz, 1H), 7.61−7.27 (m, 4H), 4.19 (d, J = 6.9 Hz, 2H), 2.16−2.04 (m, 1H), 1.42−1.02 (m, 32H), 0.98−0.70 (m, 6H).

Synthesis of 2-Amino-6-bromo-1H-benzo[de]-isoquinoline-1,3(2H)-dione (NAA-DA). 4-bromonaphthalene anhydride (2.77 g, 10 mmol) and hydrazine (1.18 g, 31 mmol) were dissolved in ethanol (30 mL) and refluxed for 4 h. Afterwards, the mixture was filtered, and the residue washed with ethanol and dried in the vacuum oven to give NAA-DA as yellow solid (2.63 g). Yield: 90%. ^{1}H NMR (DMSO-d_6, 400 MHz), δ (ppm): 8.53 (d, J = 6.5 Hz, 1H), 8.48 (d, J = 8.4 Hz, 1H), 8.29 (dd, J = 7.8, 2.1 Hz, 1H), 8.17 (dd, J = 7.9, 2.1 Hz, 1H), 8.03−7.91 (m, 1H), 5.79 (s, 2H).

Synthesis of N,N′-Diamino-1,4,5,8-naphthalenetetracarboxylic bisimide (NADA-DA). 1,4,5,8-Naphthalenetetracarboxylic dianhydride (1.34 g, 5 mmol) and hydrazine (1.18 g, 31 mmol) were dissolved in ethanol (30 mL) and refluxed for 6 h. Afterwards, the mixture was filtered, and the residue washed with ethanol and dried. After recrystallization in DMF, the product was dried to give NADA-DA as dark orange crystals (0.56 g). Yield: 38%. ^{1}H NMR (DMSO-d_6, 300 MHz), δ (ppm): 8.68 (s, 4H), 5.86 (s, 4H).

Synthesis of 2,2′-(((9-(2-octyldodecyl)-9H-carbazole-3,6-diyl)bis(methanylylidene))bis(azan-ylylidene))bis(6-bromo-1H-benzo[de]isoquinoline-1,3(2H)-dione) (NA-CANA). NAA-DA (0.21 g, 0.72 mmol) and DAODCA (0.15 g, 0.3 mmol) were dissolved in 15 mL 2-methoxyethanol and refluxed for 15 h at 80 °C. Then the reaction mixture was filtered and the residue was collected and washed with 2-methoxyethanol several times. The residue was dried in vacuum oven at 60 °C to give NACANA as light yellow solid (0.13 g). Yield: 41%. IR (KBr) ν (cm^{-1}) 1670 (C═N stretching). ^{1}H NMR ($CDCl_3$, 300 MHz), δ (ppm): 10.13 (s, 2H), 8.97−8.33 (m, 8H), 8.32−7.38 (m, 8H), 4.24 (d, J = 6.9 Hz, 2H), 2.24−2.02 (m, 1H), 1.64−0.60 (m, 38H). ^{13}C NMR (101 MHz, CDCl3) δ 191.45, 171.45, 160.71, 160.32, 145.19, 144.86, 144.17, 143.76, 133.77, 132.53, 132.32, 131.66, 131.45, 131.21, 130.90, 130.66, 130.62, 129.63, 129.32, 128.20, 128.16, 127.75, 127.61, 127.52, 124.20, 123.10, 122.98, 122.34, 122.26, 121.38, 110.07, 109.84, 77.34, 77.23, 77.03, 76.71, 48.27, 37.99, 31.85, 31.83, 29.86, 29.82, 29.59, 29.52, 29.45, 29.40, 29.32, 29.21, 29.19, 26.54, 26.51, 22.68, 22.64, 14.12. Anal. calcd for $C_{58}H_{59}Br_2N_5O_4$: C 66.35, H 5.66, N 6.67. Found: C 65.88, H 5.87, N 6.62.

Synthesis of 2,7-Bis(((9-(2-octyldodecyl)-9H-carbazol-3-yl)methylene)amino)benzo[lmn][3,8]phenanthroline-1,3,6,8(2H,7H)-tetraone (CANACA). NADA-DA (0.1 g, 0.33 mmol) and SAODCA (0.33 g, 0.69 mmol) were dissolved in 15 mL 2-methoxyethanol and refluxed for 24 h at 80 °C. Then the reaction mixture was filtered and the residue was collected and washed with 2-methoxyethanol several times. The residue was further purified through chromatography and dried in vacuum oven at 60 °C to give CANACA as red brown solid (0.11 g). Yield: 28%. IR (KBr) ν (cm^{-1}) 1668 (C═N stretching). ^{1}H NMR ($CDCl_3$, 300 MHz), δ (ppm): 10.10 (s, 2H), 8.89−8.58 (m, 6H), 8.22−7.94 (m, 4H), 7.60−7.28 (m, 8H), 4.20 (d, J = 6.9 Hz, 4H), 2.21−2.03 (m, 2H), 1.51−1.05 (m, 64H), 0.96−0.81 (m, 12H). ^{13}C NMR (101 MHz, CDCl3) δ 191.74, 172.38, 159.92, 144.55, 141.61, 131.34, 128.46, 128.41, 127.10, 126.93, 126.65, 123.91, 123.01, 122.95, 122.81, 120.66, 120.26, 109.71, 109.24, 77.34, 77.23, 77.02, 76.70, 48.07, 39.76, 39.51, 37.93, 32.57, 31.93, 31.90, 31.86, 31.84, 29.93, 29.88, 29.80, 29.64, 29.59, 29.56, 29.50, 29.45, 29.35, 29.31, 29.26, 29.22, 26.94, 26.57, 22.69, 22.64, 14.13, 14.11. Anal. calcd for $C_{80}H_{102}N_6O_4$: C 79.30, H 8.48, N 6.94. Found: C 79.04, H 8.56, N 6.98.

Memory Device Fabrication. The ITO glass was precleaned with water and then sonicated in acetone and ethanol for 20 min each. NACANA and CANACA film was fabricated from chlorobenzene (CB) solution (12 mg mL^{-1}) through spin-coating technique at a rotational speed of 1800 rpm for 40 s. The film thicknesses are estimated to be around 85 nm from the SEM images (Supporting Information Figure S7). The resulting films were dried in a vacuum oven overnight. Finally, Al top electrode was thermally evaporated onto the film surface under 2 × 10^{-6} Torr through a shadow mask with thickness around 100 nm and area of 0.20 mm^2. Scheme of the fabricated memory device is shown in Figure 1b.

3. RESULTS AND DISCUSSION

NACANA and CANACA exhibit good thermal stability with the decomposition temperature at about 300 °C, suggesting good heat resistance ability for both molecules (see Supporting Information Figure S8 and Table 1). CANACA were found quite soluble in many organic solvents such as chloroform, chlorobenzene (CB) and 1,2-dichloroethane compared to NACANA with a relatively small content of the solubilizing alkyl chain, which only shows good solubility in chlorobenzene (CB). Therefore, simple spin-coating method was employed to prepare the NACANA and CANACA thin film from chlorobenzene solution.

Table 1. Thermal, Optical, and Electrochemical Properties of the Studied A-D-A and D-A-D Molecules

compd.	T_d (°C)	λ_{max} (nm)	λ_{onset} (nm)	E_g^{opt} (eV)[a]	HOMO (eV)[b]	LUMO (eV)[c]
NACANA	290	240, 298, 351	395	3.14	−5.02	−1.88
CANACA	316	239, 290, 353	409	3.03	−5.16	−2.13

[a]Estimated from the onset absorption wavelength of the films. [b]The HOMO energy levels were obtained from cyclic voltammetry (CV) measurement with ferrocene (0.44 eV) as the reference. [c]LUMO = HOMO + band gap.

Figure 2 shows the optical absorption spectra of NACANA and CANACA nanofilms on quartz substrates. The high-energy absorption bands between 230 nm and 360 nm arise from to the $\pi-\pi^*$ transition of the conjugated backbone. The low-

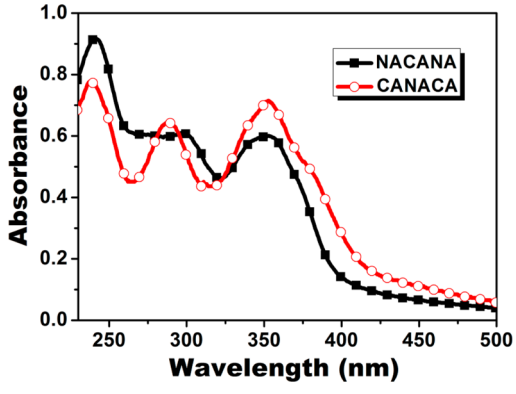

Figure 2. UV−vis spectra of the NACANA and CANACA thin films on quartz substrates.

dx.doi.org/10.1021/am405000c | ACS Appl. Mater. Interfaces 2014, 6, 94−100

energy absorption shoulders at 373 nm and 378 nm could be ascribed to the charge transfer from the carbazole donor to naphthalimide acceptor moieties in NACANA and CANACA, respectively.[21,29] With the D-A arrangement changing from A-D-A to D-A-D, an obvious bathochromic shift of the absorption band could be observed, implying a relatively strong molecular interaction in CANACA.[30] Furthermore, the absorption of the CANACA (D-A-D) at 378 nm is stronger than that of the NACANA (A-D-A), suggesting that the D-A-D arrangement may provide a larger possibility of charge transfer than the A-D-A one. The optical band gap of NACANA and CANACA can be estimated to be 3.14 eV and 3.03 eV from the onset absorption wavelength of the films, respectively.

Figure 3 shows the cyclic voltammetry (CV) measurements of NACANA and CANACA films in acetonitrile solution. Both

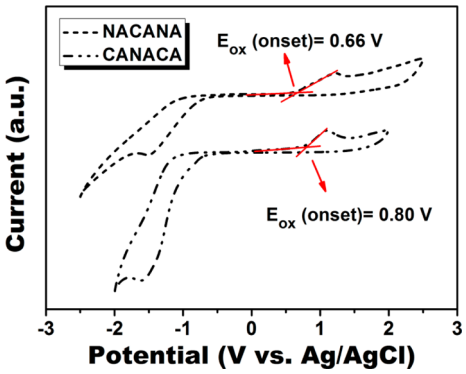

Figure 3. Cyclic voltammograms of films on ITO substrate in acetonitrile solution with the supporting electrolyte of TBAP (0.1 M). The scan rate was 100 mV s^{-1}.

NACANA and CANACA showed p-doping behavior in the anodic scan. The onset oxidation (E_{ox}^{onset}) of NACANA and CANACA is around 0.66 V and 0.80 V vs Ag/AgCl, respectively. Note that the E_{ox}^{onset} of ferrocene was measured to be 0.44 V vs Ag/AgCl in acetonitrile from the CV measurement without any organic film on the ITO glass (Supporting Information Figure S9). Assuming that the HOMO level for the F_c/F_c+ standard is −4.80 eV with respect to the zero vacuum level, the estimated highest occupied molecular orbital (HOMO) levels of NACANA and CANACA are −5.02 eV and −5.16 eV, respectively. And the determined LUMO levels of NACANA and CANACA are −1.88 eV and −2.13 eV, which were derived from the obtained optical band gap and the HOMO level.

The memory behavior of NACANA and CANACA films are demonstrated by the current−voltage (I−V) characteristics of ITO/NACANA or CANACA/Al sandwich devices. The typical I−V curves of the memory devices are shown in Figure 4. In the case of NACANA (Figure 4a), when the bias swept from 0 to −5 V (1st sweep), the device was found in the OFF state at first. When the bias reached −3.2 V, the current level underwent an abrupt increase, indicative of the transition from the original low-conductivity (OFF or "0") state to a high-conductivity (ON or "1") state. This current level transition process could serve as the "writing" process for practical data storage. The programmed ON state could be confirmed by the subsequent negative sweep (3rd sweep) and was found unable to be switched back to the initial OFF state during the reverse voltage sweep (4th sweep). The obtained ON state could maintain for ca. 12 min, after which the device would revert to the OFF state, exhibiting a volatile nature. The device could be switched on repeatedly from the relaxed OFF state (2nd and 5th sweep). The volatile behavior can be repeated at least five continuous sweeps for the same cell or devices in three different batches reproducibly. This temporary data-memorizing behavior is similar to that of a static random access memory (SRAM) device. Therefore, NACANA-based device could be applied for volatile data-storage. Figure 4c is the retention time test for the OFF and ON states of NACANA. Under a constant stress of −1 V, no obvious degradation in current level of both states is observed during the readout test for at least 200 min, indicating that the NACANA-based device possesses good stability.

Meanwhile, the memory behavior of the CANACA-based (with the D-A-D arrangement) device was also characterized, as shown in Figure 4b. The device can also be switched on during the negative sweep at threshold voltage around −3.8 V and still keeps the volatile feature. Compared to the NACANA-based device (with the A-D-A arrangement), the main difference lies in the weaker retention ability for the ON state (i.e., shorter retention time, ca. 6 min) of the CANACA-based device. The volatile behavior can be reproducibly obtained for different cells in devices from three different batches. Figure 4d shows the retention time test for the OFF and ON states of CANACA. Under a constant stress of −1 V, no obvious current degradation for both states is observed during the readout test for at least 200 min, which also suggests that CANACA-based device owns good stability.

The device performance in organic electronics is sometimes highly correlated with the surface morphology of the semiconducting active layer. To investigate the surface morphology and film microstructure, atomic force microscopy (AFM) measurements were carried out on the NACANA and CANACA films. The 3D-AFM topography images are shown in Supporting Information Figure S10. As can be seen from the AFM height images (Figure 5), NACANA film showed a relatively strong phase separation than CANACA film. However, both films are very smooth without obvious defects. The surface root-mean-square (RMS) roughness is 0.770 nm for NACANA, while CANACA has a RMS roughness of 0.426 nm. The observed smoother film of CANACA may presumably arise from the large proportion of alkyl chains incorporated in the molecule, which helps improve the quality of organic nanofilms. In order to measure the crystalline ordering within the films, X-ray diffraction (XRD) experiments were performed on the spin-coated films from chlorobenzene. As can be observed from the XRD patterns (Supporting Informaion Figure S11), both films showed obvious diffraction peaks, implying the microstructure ordering in the films. The reflections centered at ca. 2θ = 19.4° for the two films correspond to a d-spacing of ca. 4.55 Å and that at ca. 2θ = 23.8° of NACANA corresponds to a d-spacing of ca. 3.74 Å. These results suggest that both NACANA and CANACA could self-assemble into relatively ordered crystalline structure within high-quality films.[31]

To better understand the switching behavior, the electronic properties of NACANA and CANACA were studied using density function theory (DFT). Figure 6(a and b) shows the molecular orbitals and electrostatic potential (ESP) surfaces of both molecules calculated with the B3LYP/6-31G(d) basis set. The HOMOs are found to be mainly localized on the donor side (i.e., the CA moiety) and the LUMOs are mainly localized on the acceptor side (i.e., the NA moiety). This localization of HOMO/LUMO orbitals on the donor−acceptor moieties is

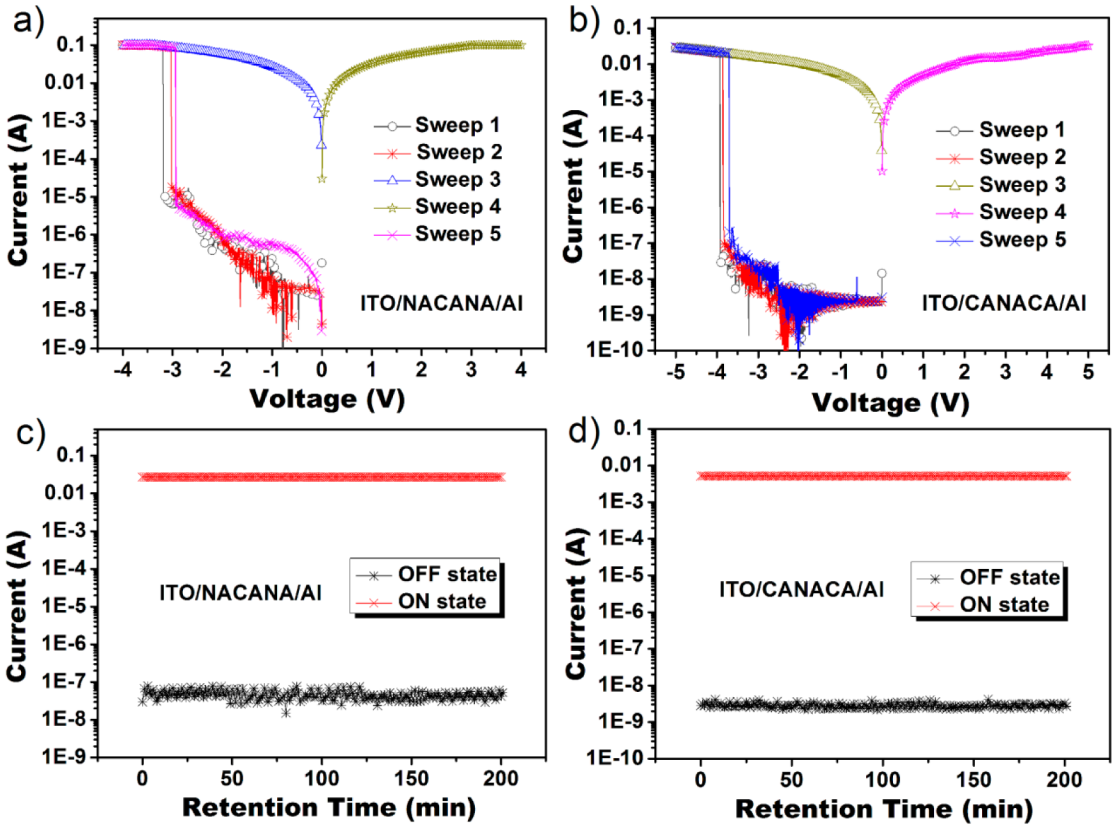

Figure 4. Current−voltage (I–V) characteristics of (a) ITO/NACANA/Al and (b) ITO/CANACA/Al memory devices; retention time measurement for the ON and OFF states of the (c) ITO/NACANA/Al and (d) ITO/CANACA/Al devices under a continuous readout voltage of −1 V.

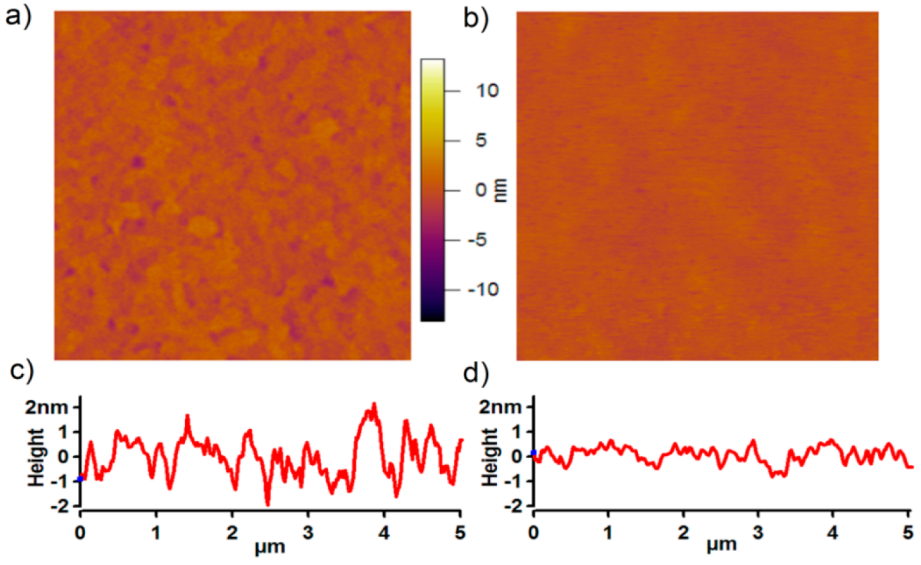

Figure 5. Tapping-mode AFM topography of NACANA (a) and CANACA (b) nanofilms; cross-section profiles of AFM topographic images of NACANA (c) and CANACA (d).

often observed in theoretical studies on D−A molecules, implying that significant charge transfer may occur in the ground-state to the excited-state transition.[25,32]

To gain insight into the switching mechanisms for the memory devices, the energy levels of NACANA and CANACA films as well as the work function of electrodes are summarized in Figure 6c. Under an applied negative bias, the energy barrier for hole injection from the bottom ITO electrode to the HOMO of NACANA and CANACA is estimated to be ca. 0.3 eV, which is much smaller compared with the electron injection barrier from the top aluminum (Al) electrode to the LUMO of the active layer (ca. 2.3 eV). Hence, hole injection is a favored process when applying a negative bias. Since these D-A molecules are not fully conjugated charge carriers mainly transport via the intermolecular hopping between neighboring molecules within the material. The DFT simulation shows

dx.doi.org/10.1021/am405000c | ACS Appl. Mater. Interfaces 2014, 6, 94−100

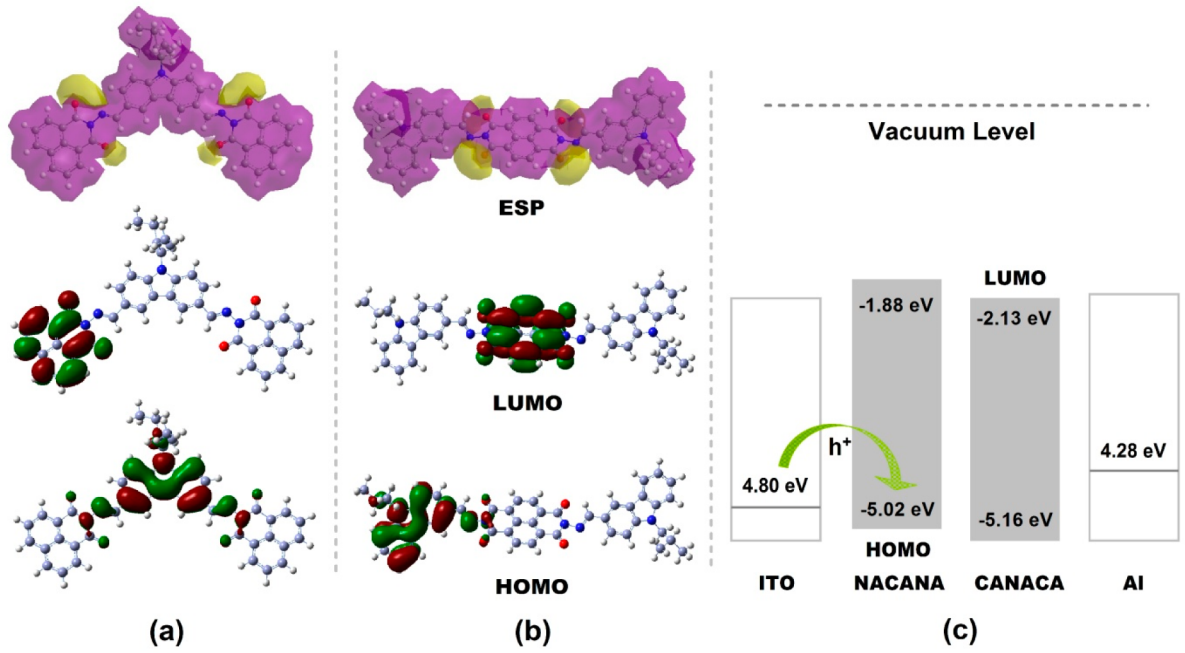

Figure 6. HOMOs, LUMOs and ESP surfaces of (a) NACANA and (b) CANACA in their optimized ground-state structures; (c) energy levels of the HOMO and LUMO of NACANA and CANACA along with the work function of the electrodes.

continuous positive ESP regions (in purple) on the molecular surfaces of NACANA and CANACA (in Figure 6a and b). These positive ESP regions can serve as an open channel for charge carrier migration throughout the conjugated backbone. The negative ESP regions (in yellow) caused by the electron-deficient groups (i.e., imide group) could function as "traps" to impede the transport of carriers. After the traps were filled, an abrupt increase in current occurred, corresponding to the OFF to ON state transition. After the external field was turned off, the trapped charges would slowly get detrapped, exhibiting the SRAM behavior.

The LUMO energy level is considered as one factor that may affect the stability of charge transfer (CT); more stable CT is often achieved with a deeper LUMO level.[33] However, in our case, CANACA with a deeper LUMO tends to have a less stable CT. These results demonstrate that the stability of CT in our case is dominated by different structures of the two molecules, which is also one crucial factor affecting the stability of CT.[34,35] The retention ability (i.e., here mainly the ON state retention time) is closely related to the acceptor's withholding ability of the trapped charges. Though the two D-A molecules both have the same imide acceptor, their difference in the D-A arrangement (D-A-D and A-D-A) renders them different charge-holding abilities. Considering the relatively shallow trap caused by the imide moiety, it is rational for both devices to exhibit the SRAM behavior, which is consistent with the previous reports.[18,24] For NACANA, the transferred electrons from the carbazole moiety can be more easily delocalized with two end-capping naphthalene rings, whereas CANACA only has one naphthalene ring at the center of the molecular backbone. The better charge delocalization of NACANA would reasonably promise a stronger withholding ability of the transported charges, therefore resulting in the longer ON-state retention time for NACANA.

4. CONCLUSIONS

Novel carbazole (CA) donor and naphthalimide (NA) acceptor based D-A molecules, NACANA and CANACA, with different D-A arrangement (A-D-A and D-A-D) were synthesized. Their photophysical and electrochemical properties, microstructure, and memory behaviors were systematically investigated. Both devices were found to exhibit the volatile nature but different retention ability for the ON state. NACANA shows an ON-state retention time (ca. 12 min) twice as long as that of CANACA (ca. 6 min). The difference in their retention ability of the programmed ON states could be assigned to the difference in the withholding ability of the trapped charges, originating from the difference of the D-A arrangement. This type of ON-state retention ability adjustment through structural design (i.e., by varying the arrangement of donor and acceptor segments) may provide a useful guide to approach tailored organic-based devices with specific data-storage properties.

■ ASSOCIATED CONTENT

Supporting Information

Scheme of the detailed synthetic route of NACANA and CANACA, FT-IR spectra, NMR spectra, SEM images, thermogravimetric analysis results, cyclic voltammogram of ferrocene, 3D-AFM topography images, and X-ray diffraction patterns of the spin-coated films. This material is available free of charge via the Internet at http://pubs.acs.org.

■ AUTHOR INFORMATION

Corresponding Author

*E-mail: lujm@suda.edu.cn (J.L.).

Notes

The authors declare no competing financial interest.

■ ACKNOWLEDGMENTS

This work was financially supported by the National Science Foundation (NSF) of China (21176164, 21206102, and

21336005), the NSF of Jiangsu Province (BE2013052), a project of the Department of Education of Jiangsu Province (12KJB430011), Suzhou Nano-project (ZXG2012023) and Project supported by the Specialized Research Fund for the Doctoral Program of Higher Education of China (Grant Nos. 20113201130003 and 20123201120005).

REFERENCES

(1) Zhuang, X. D.; Chen, Y.; Li, B. X.; Ma, D. G.; Zhang, B.; Li, Y. *Chem. Mater.* **2010**, *22*, 4455−4461.
(2) Ji, Y.; Cho, B.; Song, S.; Kim, T. W.; Choe, M.; Kahng, Y. H.; Lee, T. *Adv. Mater.* **2010**, *22*, 3071−3075.
(3) Yamamoto, T.; Zhou, Z. H.; Kanbara, T.; Shimura, M.; Kizu, K.; Maruyama, T.; Nakamura, Y.; Fukuda, T.; Lee, B. L.; Ooba, N.; Tomaru, S.; Kurihara, T.; Kaino, T.; Kubota, K.; Sasaki, S. *J. Am. Chem. Soc.* **1996**, *118*, 10389−10399.
(4) Guo, X.; Zhou, N.; Lou, S. J.; Hennek, J. W.; Ponce Ortiz, R.; Butler, M. R.; Boudreault, P.-L. T.; Strzalka, J.; Morin, P.-O.; Leclerc, M.; López Navarrete, J. T.; Ratner, M. A.; Chen, L. X.; Chang, R. P. H.; Facchetti, A.; Marks, T. J. *J. Am. Chem. Soc.* **2012**, *134*, 18427−18439.
(5) Kim, S.; Lee, J. K.; Kang, S. O.; Ko, J.; Yum, J. H.; Fantacci, S.; De Angelis, F.; Di Censo, D.; Nazeeruddin, M. K.; Grätzel, M. *J. Am. Chem. Soc.* **2006**, *128*, 16701−16707.
(6) Ponomarenko, S. A.; Kirchmeyer, S.; Elschner, A.; Huisman, B. H.; Karbach, A.; Drechsler, D. *Adv. Funct. Mater.* **2003**, *13*, 591−596.
(7) Yuan, J. Y.; Zhai, Z. C.; Dong, H. L.; Li, J.; Jiang, Z. Q.; Li, Y. Y.; Ma, W. L. *Adv. Funct. Mater.* **2013**, *23*, 885−892.
(8) Colladet, K.; Fourier, S.; Cleij, T. J.; Lusten, L.; Gelan, J.; Vanderzande, D.; Nguyen, L. H.; Neugebauer, H.; Sariciftci, S.; Aguirre, A.; Janssen, G.; Goovaerts, E. *Macromolecules* **2007**, *40*, 65−72.
(9) Bronstein, H.; Frost, J. M.; Hadipour, A.; Kim, Y.; Nielsen, C. B.; Ashraf, R. S.; Rand, B. P.; Watkins, S.; McCulloch, I. *Chem. Mater.* **2013**, *25*, 277−285.
(10) Zhuang, H.; Xu, X. P.; Liu, Y. H.; Zhou, Q. H.; Xu, X. F.; Li, H.; Xu, Q. F.; Li, N. J.; Lu, J. M.; Wang, L. H. *J. Phys. Chem. C* **2012**, *116*, 25546−25551.
(11) Shang, Y. L.; Wen, Y. Q.; Li, S. L.; Du, S. X.; He, X. B.; Cai, L.; Li, Y. F.; Yang, L. M.; Gao, H. J.; Song, Y. L. *J. Am. Chem. Soc.* **2007**, *129*, 11674−11675.
(12) Chang, J.; Ye, Q.; Huang, K. W.; Zhang, J.; Chen, Z. K.; Wu, J.; Chi, C. *Org. Lett.* **2012**, *14*, 2964−2967.
(13) Ling, Q. D.; Liaw, D. J.; Zhu, C. X.; Chan, D. S.-H.; Kang, E. T.; Neoh, K. G. *Prog. Polym. Sci.* **2008**, *33*, 917−978.
(14) Lin, J.; Ma, D. G. *Appl. Phys. Lett.* **2008**, *93*, 093505−093505-3.
(15) Zhao, F.; Liu, J. Q.; Huang, X.; Zou, X.; Lu, G.; Sun, P. J.; Wu, S. X.; Ai, W.; Yi, M. D.; Qi, X. Y.; Xie, L. H.; Wang, J. L.; Zhang, H.; Huang, W. *ACS Nano* **2012**, *6*, 3027−3033.
(16) Liu, J. Q.; Zeng, Z. Y.; Cao, X. H.; Lu, G.; Wang, L. H.; Fan, Q. L.; Huang, W.; Zhang, H. *Small* **2012**, *8*, 3517−3522.
(17) Liu, C. L.; Hsu, J. C.; Chen, W. C.; Sugiyama, K.; Hirao, A. *ACS Appl. Mater. Interfaces* **2009**, *1*, 1974−1979.
(18) Fang, Y. K.; Liu, C. L.; Yang, G. Y.; Chen, P. C.; Chen, W. C. *Macromolecules* **2011**, *44*, 2604−2612.
(19) Xie, L. H.; Ling, Q. D.; Hou, X. Y.; Huang, W. *J. Am. Chem. Soc.* **2008**, *130*, 2120−2121.
(20) Lim, S. L.; Ling, Q.; Teo, E. Y. H.; Zhu, C. X.; Chan, D. S. H.; Kang, E. T.; Neoh, K. G. *Chem. Mater.* **2007**, *19*, 5148−5157.
(21) Lee, W. Y.; Kurosawa, T.; Lin, S. T.; Higashihara, T.; Ueda, M.; Chen, W. C. *Chem. Mater.* **2011**, *23*, 4487−4497.
(22) Hahm, S. G.; Choi, S.; Hong, S.-H.; Lee, T. J.; Park, S.; Kim, D. M.; Kwon, W. S.; Kim, K.; Kim, O.; Ree, M. *Adv. Funct. Mater.* **2008**, *18*, 3276−3282.
(23) Park, S.; Kim, K.; Kim, D. M.; Kwon, W.; Choi, J.; Ree, M. *ACS Appl. Mater. Interfaces* **2011**, *3*, 765−773.
(24) Liu, Y. L.; Wang, K. L.; Huang, G. S.; Zhu, C. X.; Tok, E. S.; Neoh, K. G.; Kang, E. T. *Chem. Mater.* **2009**, *21*, 3391−3399.
(25) Zhuang, X. D.; Chen, Y.; Liu, G.; Zhang, B.; Neoh, K. G.; Kang, E. T.; Zhu, C. X.; Li, Y. X.; Niu, L. J. *Adv. Funct. Mater.* **2010**, *20*, 2916−2922.
(26) Yu, A. D.; Kurosawa, T.; Chou, Y. H.; Aoyagi, K.; Shoji, Y.; Higashihara, T.; Ueda, M.; Liu, C. L.; Chen, W. C. *ACS Appl. Mater. Interfaces* **2013**, *5*, 4921−4929.
(27) Lygaitis, R.; Getautis, V.; Grazulevicius, J. V. *Chem. Soc. Rev.* **2008**, *37*, 770−788.
(28) Ellinger, S.; Ziener, U.; Thewalt, U.; Landfester, K.; Müller, M. *Chem. Mater.* **2007**, *19*, 1070−1075.
(29) Li, H.; Jin, Z. N.; Li, N. J.; Xu, Q. F.; Gu, H. W.; Lu, J. M.; Xia, X. W.; Wang, L. H. *J. Mater. Chem.* **2011**, *21*, 5860−5862.
(30) Zhuang, H.; Zhang, Q. J.; Zhu, Y. X.; Xu, X. F.; Liu, H. F.; Li, N. J.; Xu, Q. F.; Li, H.; Lu, J. M.; Wang, L. H. *J. Mater. Chem. C* **2013**, *1*, 3816−3824.
(31) Loser, S.; Bruns, C. J.; Miyauchi, H.; Ortiz, R. P.; Facchetti, A.; Stupp, S. I.; Marks, T. J. *J. Am. Chem. Soc.* **2011**, *133*, 8142−8145.
(32) Marsden, J. A.; Miller, J. J.; Shirtcliff, L. D.; Haley, M. M. *J. Am. Chem. Soc.* **2005**, *127*, 2464−2476.
(33) Kuorosawa, T.; Lai, Y. C.; Higashihara, T.; Ueda, M.; Liu, C. L.; Chen, W. C. *Macromolecules* **2012**, *45*, 4556−4563.
(34) Li, H. Y.; Batsanov, A. S.; Moss, K. C.; Vaughan, H. L.; Dias, F. B.; Kamtekar, K. T.; Bryce, M. R.; Monkman, A. P. *Chem. Commun.* **2010**, *46*, 4812−4814.
(35) Kuorosawa, T.; Chueh, C. C.; Liu, C. L.; Higashihara, T.; Ueda, M.; Chen, W. C. *Macromolecules* **2010**, *43*, 1236−1244.